Sr_2MoO_4 and Sr_2RuO_4: Disentangling the Roles of Hund's and van Hove Physics

Jonathan Karp,[1,*] Max Bramberger,[2,3] Martin Grundner,[2,3] Ulrich Schollwöck,[2,3]
Andrew J. Millis,[4,5] and Manuel Zingl[5]

[1]*Department of Applied Physics and Applied Math, Columbia University, New York, New York 10027, USA*
[2]*Arnold Sommerfeld Center of Theoretical Physics, Department of Physics, University of Munich, Theresienstrasse 37, 80333 Munich, Germany*
[3]*Munich Center for Quantum Science and Technology (MCQST), Schellingstrasse 4, 80799 Munich, Germany*
[4]*Department of Physics, Columbia University, New York, New York 10027, USA*
[5]*Center for Computational Quantum Physics, Flatiron Institute, 162 5th Avenue, New York, New York 10010, USA*

(Received 9 May 2020; accepted 22 September 2020; published 12 October 2020)

Sr_2MoO_4 is isostructural to the unconventional superconductor Sr_2RuO_4 but with two electrons instead of two holes in the Mo/Ru-t_{2g} orbitals. Both materials are Hund's metals, but while Sr_2RuO_4 has a van Hove singularity in close proximity to the Fermi surface, the van Hove singularity of Sr_2MoO_4 is far from the Fermi surface. By using density functional plus dynamical mean-field theory, we determine the relative influence of van Hove and Hund's metal physics on the correlation properties. We show that theoretically predicted signatures of Hund's metal physics occur on the occupied side of the electronic spectrum of Sr_2MoO_4, identifying Sr_2MoO_4 as an ideal candidate system for a direct experimental confirmation of the theoretical concept of Hund's metals via photoemission spectroscopy.

DOI: 10.1103/PhysRevLett.125.166401

Sr_2RuO_4 has emerged as an exemplary quantum material, providing fundamental insight into the effect of electronic correlations on material properties [1–14]. The rich electronic properties of Sr_2RuO_4 are determined by a sophisticated interplay of factors, including the on-site Coulomb repulsion, spin-orbit coupling, and a van Hove singularity, but it is believed that the nontrivial physics of the interorbital Hund's interaction [15–23] is at the heart of the strongly correlated nature of this material [11,23–25]. However, unambiguous experimental observation of Hund's-related physics has been challenging. For example, the presence of a van Hove singularity in the vicinity of the Fermi level impacts electronic correlations, masking the effects of the Hund's coupling on the quasiparticle mass enhancement [11,24,25]. While Hund's physics has been predicted to produce a characteristic peak in the single-particle spectrum [21,22,26], for Sr_2RuO_4 this peak occurs on the unoccupied side of the spectrum [4,10,13]. Thus, a direct experimental observation with conventional photoemission spectroscopy is challenging, though indirect hints have been seen in optical conductivity [4].

In this Letter, we use a combination of density functional theory (DFT) and dynamical mean-field theory (DMFT) to argue that Sr_2MoO_4, a material isostructural to Sr_2RuO_4 but with a different electron count, provides an ideal platform to study Hund's physics in quantum materials, while the comparison to Sr_2RuO_4 provides insight into the role of van Hove singularities. We show that (i) the characteristic Hund's metal peak appears on the occupied side of the electronic spectrum for Sr_2MoO_4, making it directly observable in conventional photoemission experiments, unlike for Sr_2RuO_4 where the peak is on the unoccupied side, and (ii) in contrast to Sr_2RuO_4, for Sr_2MoO_4 the van Hove singularity is substantially displaced from the Fermi surface, permitting the effects of van Hove and Hund's physics to be disentangled.

Sr_2MoO_4 crystallizes in the same tetragonal $I4/mmm$ crystal structure as Sr_2RuO_4, with $a = b$ and c lattice parameters being slightly larger in Sr_2MoO_4, as expected from the larger ionic radius of Mo^{4+} in comparison to Ru^{4+} [27–29]. The octahedral oxygen environment surrounding the Ru/Mo atoms leads to an $e_g - t_{2g}$ splitting of the Ru/Mo-4d shell with unoccupied e_g orbitals and three t_{2g} orbitals occupied by 2 electrons in Sr_2MoO_4 and 4 electrons in Sr_2RuO_4. Two decades ago, Sr_2MoO_4 was synthesized in polycrystalline form [27–29], and later, 60 unit cell single-crystal films were reported [30]. In contrast to the vast literature on Sr_2RuO_4, only the basic electronic structure of Sr_2MoO_4 has been studied with DFT [31]. We hope that the results presented here will kindle experimental interest.

Figure 1 shows the DFT (one electron) electronic structure calculated with WIEN2k [32] using the Perdew–Burke-Ernzerhof form of the Generalized Gradient Approximation (PBE-GGA) [33] exchange-correlation functional and experimental atomic positions [31,34], along with Wannier bands calculated with Wannier90 [46,47] and discussed below. The insets of Fig. 1 show the Fermi surfaces, which consist of three sheets: two electronlike sheets centered at Γ and one holelike pocket

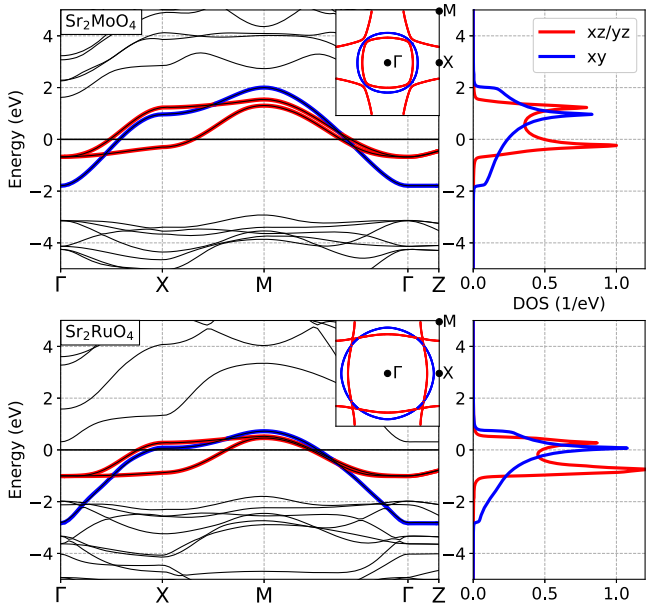

FIG. 1. Left: comparison of DFT (black) and xy (blue) and xz/yz-derived (red) Wannier bands for Sr_2MoO_4 (top) and Sr_2RuO_4 (bottom). Insets: Fermi surfaces in the $k_z = 0$ plane. Right: orbitally resolved Wannier densities of states (per spin).

centered at the M point. The electron sheets are smaller and the hole pockets are larger in Sr_2MoO_4 than in Sr_2RuO_4, due to the lower electron count of Sr_2MoO_4. Without spin-orbit coupling, the smaller electron sheet and the hole-pockets are of pure xz/yz character (red), whereas the larger electron sheet is of xy orbital character (blue).

The inclusion of spin-orbit coupling, which is slightly smaller in Sr_2MoO_4 (80 meV) than in Sr_2RuO_4 (100 meV), leads to a momentum-dependent mixing of the orbital character of the Fermi surface sheets [6,8,48]. In contrast to Sr_2RuO_4, the spin-orbit coupling does not cause a restructuring of the Fermi surface in Sr_2MoO_4. We discuss the electronic structure with spin-orbit coupling in the Supplemental Material [34], but we neglect it for most of this work as it is not important for the Hund's-related electronic correlations, which are of primary interest here.

To capture the effect of electronic correlations at low energies, we construct a basis of three t_{2g}-like maximally localized Wannier orbitals [49,50]. As shown in the left-hand panels of Fig. 1, the Wannier states (colored) reproduce the DFT bands (black) very precisely in both materials. We note that for Sr_2MoO_4 the t_{2g}-derived bands around the Fermi energy are separated from the O-p states by more than 1 eV, which makes the selection of a low-energy subspace even more natural. The shape of the Wannier orbital density of states (DOS), Fig. 1 right-hand panels, is a result of the quasi-2D crystal structure, which makes the rather 2D-like xy orbital (blue) different from the more 1D xz/yz ones (red). For Sr_2MoO_4 the degenerate xz/yz orbitals have a wider bandwidth (2.2 eV) than for Sr_2RuO_4 (1.5 eV), but the difference in bandwidths of the xy orbital is less (3.6 eV versus 3.8 eV). Overall, the band structures and DOS of the two materials are very similar apart from a shift in the Fermi level due to the different electron count. For the xz/yz orbitals this results in the upper band-edge singularity being closer to the Fermi level for Sr_2RuO_4 and the lower one being closer to the Fermi level for Sr_2MoO_4. There is another important qualitative difference: For Sr_2MoO_4 the saddle point of the xy-derived band at the X point, corresponding to a van Hove singularity in the DOS, is at $\sim$1 eV above the Fermi energy, while for Sr_2RuO_4 it is in close proximity to the Fermi energy. We will see in the following how this key difference in the electronic structure impacts the strength of electronic correlations.

We include the effect of electron-electron correlations by adding local interactions of Hubbard-Kanamori form [51] using a Coulomb repulsion $U = 2.3$ eV and a Hund's coupling $J = 0.4$ eV [52] and solving the resulting problem within single-site DMFT [54–56]. We obtain results at nonzero temperatures ranging from 29 to 464 K "by employing the continuous time quantum Monte Carlo method in the hybridization expansion (CTHYB) [57,58] as the impurity solver and at effectively zero temperature using a matrix product states (MPS) based solver [53,59].

We characterize the strength of electronic correlations by the inverse quasiparticle renormalization $Z^{-1} = 1 - \partial \mathrm{Re}\Sigma(\omega \to 0)/\partial\omega$ [34] related, in the single-site DMFT approximation, to the quasiparticle mass enhancement as $m^\star/m = Z^{-1}$, shown in Fig. 2. For both materials the calculated low-temperature mass enhancements agree with experimental specific heat measurements, which indicate that the overall mass enhancement of Sr_2RuO_4 is about 4 [3,6,60], while for Sr_2MoO_4 correlations are weaker and result in a mass enhancement of only around 2 [29,31]. From the specific heat $c_p \sim \sum_l (m^*/m)_l N_l(E_F)$, where $l \in \{xy, xz, yz\}$ and $N_l(E_F)$ is the bare DOS at the Fermi energy, we obtain a specific heat ratio $c_p^{\mathrm{SRO}}/c_p^{\mathrm{SMO}} = 2.4$, which is in good agreement with the experimental value of about 2.8 [29].

At zero temperature, the xz/yz orbital mass enhancements of the two materials are approximately in the same ratio as the inverses of the respective bandwidths. We attribute this finding to the nearly symmetrical shape of the xz/yz DOS in both materials; see Fig. 1. The situation for the xy orbital is different: For Sr_2RuO_4, in agreement with previous works [24,25], we find that even though the xy orbital has the larger bandwidth, its mass enhancement is nearly twice as large as the mass enhancement of the xz/yz orbitals. The unusually large xy orbital mass enhancement of Sr_2RuO_4 has been attributed to the proximity of the van Hove singularity to the chemical potential [24,25]. Conversely, for Sr_2MoO_4 the van Hove singularity is far removed from the chemical potential, and the mass enhancements are consistent with the difference in the bare bandwidths; the xy orbital is substantially less correlated than the xz/yz orbitals. As Sr_2RuO_4 is

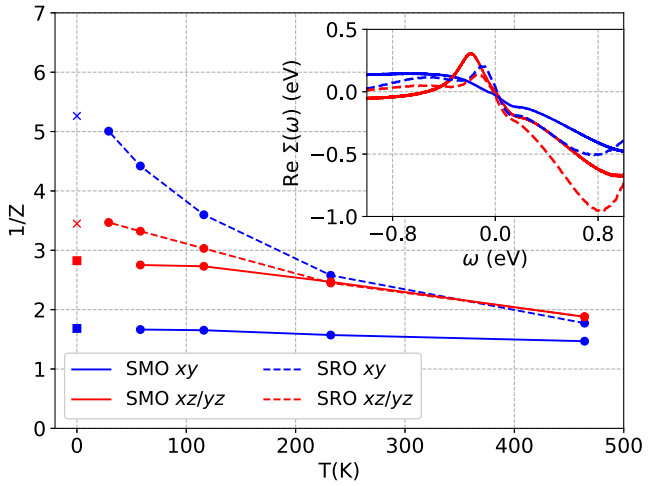

FIG. 2. Main: DMFT mass enhancement parameters $1/Z$ [34] for the xy (blue) and xz/yz (red) orbitals of Sr_2MoO_4 (solid lines) and Sr_2RuO_4 (dashed lines) as a function of temperature. The error bars of the CTHYB results (circles) are smaller than the marker size. The zero temperature values (squares and crosses) have been obtained using a matrix product states impurity solver [34,53,59]. Inset: real part of the DMFT real-frequency self-energies obtained at $T = 232$ K using CTHYB as the impurity solver and with subsequent analytic continuation to the real-frequency axis [34,54,57,61]. Note that the chemical potential has also been subtracted. For Sr_2RuO_4 (dashed lines) we show the negative of the reflection of the self-energies through $\omega = 0$; i.e., $-\Sigma(-\omega)$.

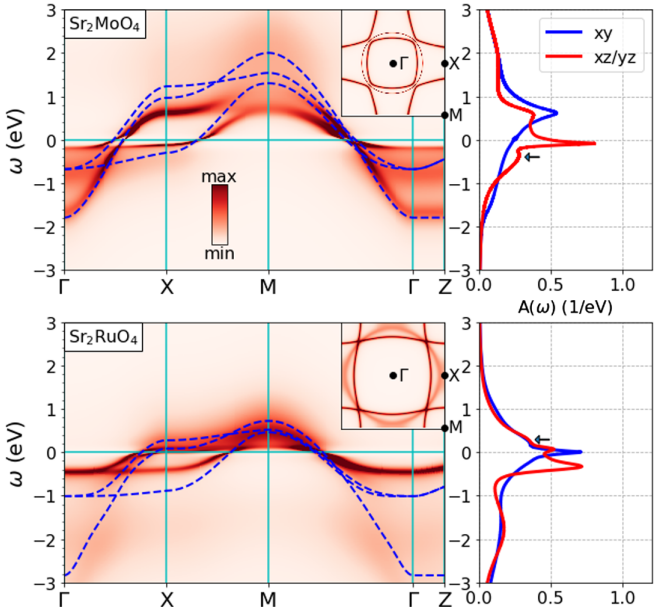

FIG. 3. Many-body electronic structure obtained with DMFT for Sr_2MoO_4 (top panels) and Sr_2RuO_4 (bottom panels) at $T = 232$ K. Left: momentum-resolved spectral function $A_k(\omega)$ (false color) along a high-symmetry k path through the Brillouin zone compared to the Wannier bands (dashed blue lines). Insets: spectral function $A_k(\omega = 0)$ in the $k_z = 0$ plane. Right: momentum-integrated spectral function $A(\omega)$ (per spin) for the xy (blue) and the xz/yz (red) orbitals. Black arrows point to the Hund's peaks. Note the different range of energy in comparison to Fig. 1.

cooled, the mass enhancements exhibit a strong temperature and orbital dependence with no sign of saturation above 30 K. This is in accordance with a Fermi liquid temperature of about 25 K [25,60]. For Sr_2MoO_4, we observe only a weak temperature dependence of the mass enhancement, and its saturation at about 100 K indicates a much higher Fermi liquid coherence scale than in Sr_2RuO_4. These findings suggest that the van Hove singularity provokes a suppression of the Fermi liquid temperature in Sr_2RuO_4 and demonstrate the importance of capturing the interplay of correlation physics and specifics of band structure to understand the quasiparticle properties in strongly correlated materials.

In contrast to the van Hove singularity, the spin-orbit coupling does not influence the mass enhancements of Sr_2RuO_4 [13,53]. However, it is known from theory and experiment that electronic correlations lead to an effective spin-orbit coupling 2 times larger than its bare value [6,12,13,53,62]. By using the MPS-based impurity solver for calculations with spin-orbit coupling, we find that the same picture holds in Sr_2MoO_4, yielding a slightly higher enhancement factor of about 2.5 (see Supplemental Material [34]). We therefore conclude that the correlation-enhanced spin-orbit coupling in both materials is to a large degree a result of local interactions [62] rather than a consequence of van Hove physics.

The materials' similarities and differences are also evident in the correlated spectral function, shown in the left-hand panel of Fig. 3. We see that for Sr_2RuO_4, the unoccupied states conform closely to the bare bands, while the occupied bands are shifted substantially toward the chemical potential. For Sr_2MoO_4, the renormalization is less severe, and the unoccupied states differ considerably from the DFT bands. In the insets of Fig. 3, we show the spectral function at $T = 232$ K and $\omega = 0$ in the $k_z = 0$ plane, practically a many-body version of the Fermi surfaces of Fig. 1 at finite temperature. These many-body Fermi surfaces portray the major differences found in the xy orbitals. While the xy sheet is very sharp in Sr_2MoO_4, we find it to be broadened in Sr_2RuO_4. This is caused by the van Hove singularity in Sr_2RuO_4, which is shifted even closer to the chemical potential due to electronic correlations.

Results for the orbitally resolved self-energies at $T = 232$ K are presented in the inset of Fig. 2. Note that for Sr_2RuO_4 what is shown is the negative of the reflection of the self-energy through $\omega = 0$; i.e., $-\Sigma(-\omega)$. The xz/yz self-energies for the two materials have a clear qualitative similarity, showing that for these orbitals Sr_2MoO_4 is—to a good approximation—indeed the particle-hole dual of Sr_2RuO_4. The self-energies have a negative slope at $\omega = 0$, corresponding to the usual low-energy reduction

of the quasiparticle velocity due to strong correlations. There is, however, an interesting inversion of slope around $\omega = -0.2$ eV, which has been pointed out in several DMFT works on Sr_2RuO_4 [4,13,25,63]. For Sr_2MoO_4 the inversion of slope is only present in the xz/yz self-energy.

The inversion of slope occurs still well within the bare bandwidth, and may lead to a "retracted" renormalization of the quasiparticle dispersion. The consequence is an additional side peak in the spectral function $A(\omega)$ (marked with small arrows in Fig. 3, right-hand panels), which cannot be related to a structure present in the noninteracting DOS. Model system calculations indicate that the inverted slope and the corresponding side peak in $A(\omega)$ are characteristic signatures of the spin-orbital separation occurring in Hund's metals [20–22]. For Sr_2MoO_4, with two electrons in three orbitals, the screening of the orbital degrees of freedom requires binding a conduction band electron to the correlated site, resulting in the formation of a large $S = 3/2$ local moment [21]. Breaking this composite spin requires the removal of an electron, and thus an excitation corresponding to the energy of this process can be expected in the electron-removal part of the spectrum. Conversely, for Sr_2RuO_4 with a more than half-filled shell, i.e., four electrons in three orbitals, the screening involves an additional hole, and thus the Hund's metal side peak is found at positive energies.

To our knowledge, no photoemission experiment has yet observed this side peak, probably because most studied Hund's metals have more than half-filled correlated shells so the Hund's peak is on the unoccupied side of the spectrum and not observable in photoemission. Crucially, for Sr_2MoO_4 the Hund's metal peak is present on the occupied side and therefore observable in photoemission. However, in the momentum-integrated spectral function $A(\omega)$, the Hund's metal peak is a relatively weak feature. We therefore show here how an exploration of the momentum dependence of the spectral function also reveals the importance of Hund's physics.

Examination of Fig. 3 shows that for Sr_2MoO_4 along the Γ-X path, there are two pronounced spectral features on the occupied side, one at -0.2 eV corresponding to the renormalized xz/yz-derived bands and another corresponding to the strongly dispersing xy-derived band. Between these two is additional spectral weight which corresponds to the Hund's metal excitation (see also Supplemental Material [34]). The Hund's metal spectral weight roughly follows the energy of the lower noninteracting xz/yz-derived band. We also see that the occupied side of $A_k(\omega)$ of Sr_2MoO_4 is very different from that of Sr_2RuO_4. The latter shows strongly renormalized xz/yz-derived bands and a very incoherent xy quasiparticle dispersion only visible around zero energy close to the X point. For Sr_2RuO_4 the Hund's metal physics is responsible for the weight on the unoccupied side above $\sim$0.3 eV on the X-M path.

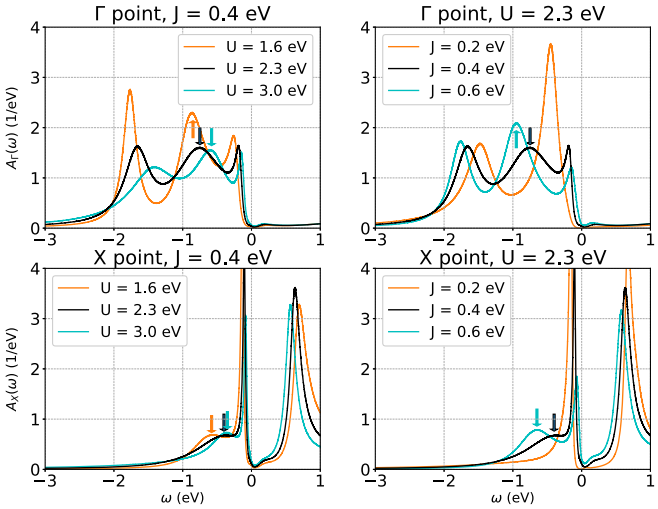

FIG. 4. DMFT spectral function of Sr_2MoO_4 at the Γ point (top row) and the X point (bottom row) for different values of U at fixed $J = 0.4$ eV (left-hand panels) and for different values of J at fixed $U = 2.3$ eV (right-hand panels) calculated at $T = 232$ K. Arrows point to the Hund's peaks.

In Fig. 4 we examine the Hund's peak physics in more detail by focusing on the energy dependence of the spectrum at two characteristic momentum points. Concentrating first on the Γ point, for the parameters believed to be relevant to Sr_2MoO_4 and Sr_2RuO_4, a distinct three-peak structure is observed on the occupied side of the spectrum (black line). Following our discussion above, the peak closest to the chemical potential stems from the strong renormalization of the bare xz/yz bands, the peak furthest from the chemical potential results from the xy orbital, and the peak in the middle is a direct consequence of the Hund's metal nature of Sr_2MoO_4. Based on our calculations, the three peaks are well separated and the intensity of the Hund's metal peak is similar to the intensity of the other two peaks.

Changing the Coulomb repulsion or Hund's coupling away from the physically expected values changes the behavior. At fixed U the Hund's peak shifts away from the chemical potential with increasing J (right-hand panel), while at fixed J it shifts toward the chemical potential when U is increased (left-hand panel). Increasing J/U will favor the formation of a composite $S = 3/2$ impurity spin, leading to an increased coherence energy scale for the orbital screening process, and thus the Hund's metal peak likewise moves to higher (negative) energies. Of course, the three-peak structure is only present for parameters within the Hund's metal regime. For too small J/U the three-peak structure ceases to exist, as is indeed the case for $U = 2.3$ eV and $J = 0.2$ eV; see Fig. 4, right-hand panel. We see similar behavior at the X point (Fig. 4, bottom panels), although the Hund's side peak is much less pronounced than at the Γ point. For $U = 2.3$ eV and $J = 0.4$ eV (black lines), we find a small Hund's side peak at

$\omega \sim -0.5$ eV. The peak moves closer to the chemical potential for increasing U (left-hand panel), while the peak moves in the opposite direction for increasing J. For $J = 0.2$ eV the peak disappears entirely.

We remark that the calculated dependence on U and J excludes that the observed peak originates from the atomic multiplet structure because the multiplet splitting would evolve in the opposite way as J is varied. The multiplet structure has been used to determine J, for example, in the Mott-insulating state of Ca_2RuO_4, resulting in the same Hund's coupling as used in this work: $J = 0.4$ eV [64]. Our work shows that the position of the Hund's peak can provide information on the interaction strength in a material which is metallic and where the atomic multiplet structure is not experimentally visible.

In addition to the single-particle quantities discussed here, we also calculate the probabilities of different local configurations of the correlated Ru/Mo site (see Supplemental Material [34]). We find that the probability that the site is in a locally high-spin configuration is almost the same in the two compounds, indicating a strong similarity of the local magnetic correlations.

In this Letter we have presented a study of the correlated electronic structure of Sr_2MoO_4 in comparison with that of the well-understood material Sr_2RuO_4. The difference in electron density (2 electrons per Mo versus 4 per Ru) leads to similarities (in many respects Sr_2MoO_4 is the particle-hole dual of Sr_2RuO_4) but also to pronounced differences in physics, which can be used to gain understanding of the interplay between correlated electron physics and band structure aspects. For Sr_2MoO_4 the van Hove singularity is far from the chemical potential, while for Sr_2RuO_4 it is very close. A comparison of the two materials therefore provides insight into the importance of van Hove physics in Hund's metals. Perhaps of more fundamental significance, for Sr_2MoO_4 the characteristic spectral features theoretically predicted to arise in Hund's metals occur on the occupied side of the electronic spectrum and should therefore be accessible to photoemission experiments. Single-crystal Sr_2MoO_4 thin films have been synthesized [30], allowing for angle-resolved measurements. Sr_2MoO_4 is thus an ideal system for direct experimental tests of the novel aspects of Hund's metal physics. Further, an experimental observation of the Hund's metal peak in Sr_2MoO_4 would open the intriguing possibility to experimentally determine J/U in a metallic system.

In Sr_2MoO_4 no superconductivity has been found to date. Nevertheless, we believe that future studies of this material could bring key insight on the importance of Hund's physics, spin-orbit coupling, the van Hove singularity, and other band structure details for the emergence of unconventional superconductivity in Sr_2RuO_4. To this end, the future study of multiparticle physics in Sr_2MoO_4, similar to recent works on Sr_2RuO_4 [14,65–67], is desirable.

We thank A. Georges, G. Kotliar, and J. Mravlje for fruitful discussions. J. K. and A. J. M. acknowledge funding by the Materials Sciences and Engineering Division, Basic Energy Sciences, Office of Science, U.S. DOE. M. B., M. G., and U.S. acknowledge support by the Deutsche Forschungsgemeinschaft (DFG, German Research Foundation) under Germany's Excellence Strategy-426 EXC-2111-390814868 and by Research Unit FOR 1807 under Project No. 207383564. M. B., M. G., and U.S. thank the Flatiron Institute for its hospitality. The Flatiron Institute is a division of the Simons Foundation.

*jk3986@columbia.edu

[1] A. P. Mackenzie, S. R. Julian, A. J. Diver, G. G. Lonzarich, N. E. Hussey, Y. Maeno, S. Nishizaki, and T. Fujita, Physica (Amsterdam) **263C**, 510 (1996).
[2] Y. Maeno, K. Yoshida, H. Hashimoto, S. Nishizaki, S.-I. Ikeda, M. Nohara, T. Fujita, A. P. Mackenzie, N. E. Hussey, J. G. Bednorz, and F. Lichtenberg, J. Phys. Soc. Jpn. **66**, 1405 (1997).
[3] C. Bergemann, A. P. Mackenzie, S. R. Julian, D. Forsythe, and E. Ohmichi, Adv. Phys. **52**, 639 (2003).
[4] D. Stricker, J. Mravlje, C. Berthod, R. Fittipaldi, A. Vecchione, A. Georges, and D. van der Marel, Phys. Rev. Lett. **113**, 087404 (2014).
[5] M. Behrmann, C. Piefke, and F. Lechermann, Phys. Rev. B **86**, 045130 (2012).
[6] A. Tamai, M. Zingl, E. Rozbicki, E. Cappelli, S. Riccò, A. de la Torre, S. McKeown Walker, F. Y. Bruno, P. D. C. King, W. Meevasana, M. Shi, M. Radović, N. C. Plumb, A. S. Gibbs, A. P. Mackenzie, C. Berthod, H. U. R. Strand, M. Kim, A. Georges, and F. Baumberger, Phys. Rev. X **9**, 021048 (2019).
[7] X. Deng, K. Haule, and G. Kotliar, Phys. Rev. Lett. **116**, 256401 (2016).
[8] C. N. Veenstra, Z. H. Zhu, M. Raichle, B. M. Ludbrook, A. Nicolaou, B. Slomski, G. Landolt, S. Kittaka, Y. Maeno, J. H. Dil, I. S. Elfimov, M. W. Haverkort, and A. Damascelli, Phys. Rev. Lett. **112**, 127002 (2014).
[9] M. Zingl, J. Mravlje, M. Aichhorn, O. Parcollet, and A. Georges, npj Quantum Mater. **4**, 35 (2019).
[10] E. Sarvestani, G. Zhang, E. Gorelov, and E. Pavarini, Phys. Rev. B **97**, 085141 (2018).
[11] H. J. Lee, C. H. Kim, and A. Go, arXiv:2002.04825.
[12] G. Zhang, E. Gorelov, E. Sarvestani, and E. Pavarini, Phys. Rev. Lett. **116**, 106402 (2016).
[13] M. Kim, J. Mravlje, M. Ferrero, O. Parcollet, and A. Georges, Phys. Rev. Lett. **120**, 126401 (2018).
[14] H. U. R. Strand, M. Zingl, N. Wentzell, O. Parcollet, and A. Georges, Phys. Rev. B **100**, 125120 (2019).
[15] Z. P. Yin, K. Haule, and G. Kotliar, Nat. Mater. **10**, 932 (2011).
[16] L. de' Medici, J. Mravlje, and A. Georges, Phys. Rev. Lett. **107**, 256401 (2011).
[17] A. Georges, L. de' Medici, and J. Mravlje, Annu. Rev. Condens. Matter Phys. **4**, 137 (2013).

[18] N. Lanatà, H. U. R. Strand, G. Giovannetti, B. Hellsing, L. de' Medici, and M. Capone, Phys. Rev. B **87**, 045122 (2013).

[19] L. Fanfarillo and E. Bascones, Phys. Rev. B **92**, 075136 (2015).

[20] K. M. Stadler, Z. P. Yin, J. von Delft, G. Kotliar, and A. Weichselbaum, Phys. Rev. Lett. **115**, 136401 (2015).

[21] K. Stadler, G. Kotliar, A. Weichselbaum, and J. von Delft, Ann. Phys. (Amsterdam) **405**, 365 (2019).

[22] A. Horvat, R. Zitko, and J. Mravlje,arXiv:1907.07100.

[23] X. Deng, K. M. Stadler, K. Haule, A. Weichselbaum, J. von Delft, and G. Kotliar, Nat. Commun. **10**, 2721 (2019).

[24] J. Mravlje, M. Aichhorn, T. Miyake, K. Haule, G. Kotliar, and A. Georges, Phys. Rev. Lett. **106**, 096401 (2011).

[25] F. B. Kugler, M. Zingl, H. U. R. Strand, Seung-Sup B. Lee, J. von Delft, and A. Georges, Phys. Rev. Lett. **124**, 016401 (2020).

[26] H. Wadati, J. Mravlje, K. Yoshimatsu, H. Kumigashira, M. Oshima, T. Sugiyama, E. Ikenaga, A. Fujimori, A. Georges, A. Radetinac, K. S. Takahashi, M. Kawasaki, and Y. Tokura, Phys. Rev. B **90**, 205131 (2014).

[27] N. Shirakawa and S. Ikeda, Physica (Amsterdam) **364C**, 309 (2001).

[28] N. Shirakawa, S.-I. Ikeda, H. Matsuhata, and H. Bando, Jpn. J. Appl. Phys. **40**, L741 (2001).

[29] S.-I. Ikeda, N. Shirakawa, H. Bando, and Y. Ootuka, J. Phys. Soc. Jpn. **69**, 3162 (2000).

[30] A. Radetinac, K. Takahashi, L. Alff, M. Kawasaki, and Y. Tokura, J. Cryst. Growth **322**, 38 (2011).

[31] I. Hase, S.-I. Ikeda, N. Shirakawa, and J. K. Stalick, J. Low Temp. Phys. **131**, 269 (2003).

[32] P. Blaha, K. Schwarz, G. K. H. Madsen, D. Kvasnicka, J. Luitz, R. Laskowski, F. Tran, and L. D. Marks, *WIEN2k, An augmented plane wave+local orbitals program for calculating crystal properties*, edited by K. Schwarz (Techniche Universität, Wien, 2018).

[33] J. P. Perdew, K. Burke, and M. Ernzerhof, Phys. Rev. Lett. **77**, 3865 (1996).

[34] See Supplemental Material at http://link.aps.org/supplemental/10.1103/PhysRevLett.125.166401 for which provides additional details on the calculations and more detail on the effect of SOC, which contains the Refs. [35–45].

[35] R. Bulla, A. C. Hewson, and T. Pruschke, J. Phys. Condens. Matter **10**, 8365 (1998).

[36] J. Haegeman, J. I. Cirac, T. J. Osborne, I. Pižorn, H. Verschelde, and F. Verstraete, Phys. Rev. Lett. **107**, 070601 (2011).

[37] J. Haegeman, C. Lubich, I. Oseledets, B. Vandereycken, and F. Verstraete, Phys. Rev. B **94**, 165116 (2016).

[38] S. Paeckel, T. Köhler, A. Swoboda, S. R. Manmana, U. Schollwöck, and C. Hubig, Ann. Phys. (Amsterdam) **411**, 167998 (2019).

[39] T. Barthel, U. Schollwöck, and S. R. White, Phys. Rev. B **79**, 245101 (2009).

[40] M. Caffarel and W. Krauth, Phys. Rev. Lett. **72**, 1545 (1994).

[41] T. Vogt and D. J. Buttrey, Phys. Rev. B **52**, R9843 (1995).

[42] L. Vaugier, H. Jiang, and S. Biermann, Phys. Rev. B **86**, 165105 (2012).

[43] C. Hubig, Symmetry-protected tensor networks, Ph. D. thesis, Ludwig-Maximilians-Universität München, 2017.

[44] C. Hubig, F. Lachenmaier, N.-O. Linden, T. Reinhard, L. Stenzel, A. Swoboda, and M. Grundner, The SYTEN toolkit, https://syten.eu.

[45] G. J. Kraberger, R. Triebl, M. Zingl, and M. Aichhorn, Phys. Rev. B **96**, 155128 (2017).

[46] J. Kuneš, R. Arita, P. Wissgott, A. Toschi, H. Ikeda, and K. Held, Comput. Phys. Commun. **181**, 1888 (2010).

[47] A. A. Mostofi, J. R. Yates, Y.-S. Lee, I. Souza, D. Vanderbilt, and N. Marzari, Comput. Phys. Commun. **178**, 685 (2008).

[48] M. W. Haverkort, I. S. Elfimov, L. H. Tjeng, G. A. Sawatzky, and A. Damascelli, Phys. Rev. Lett. **101**, 026406 (2008).

[49] N. Marzari and D. Vanderbilt, Phys. Rev. B **56**, 12847 (1997).

[50] I. Souza, N. Marzari, and D. Vanderbilt, Phys. Rev. B **65**, 035109 (2001).

[51] J. Kanamori, Prog. Theor. Phys. **30**, 275 (1963).

[52] For simplicity we use the same interaction parameters in both compounds. These values are commonly used for Sr_2RuO_4 [4,9,13,14,24,53]. Following constrained random phase calculations, we note that in Sr_2MoO_4 the interaction values are estimated to be about 8% larger than in Sr_2RuO_4 [42].

[53] N.-O. Linden, M. Zingl, C. Hubig, O. Parcollet, and U. Schollwöck, Phys. Rev. B **101**, 041101(R) (2020).

[54] O. Parcollet, M. Ferrero, T. Ayral, H. Hafermann, I. Krivenko, L. Messio, and P. Seth, Comput. Phys. Commun. **196**, 398 (2015).

[55] A. Georges, G. Kotliar, W. Krauth, and M. J. Rozenberg, Rev. Mod. Phys. **68**, 13 (1996).

[56] M. Aichhorn, L. Pourovskii, P. Seth, V. Vildosola, M. Zingl, O. E. Peil, X. Deng, J. Mravlje, G. J. Kraberger, C. Martins, M. Ferrero, and O. Parcollet, Comput. Phys. Commun. **204**, 200 (2016).

[57] P. Seth, I. Krivenko, M. Ferrero, and O. Parcollet, Comput. Phys. Commun. **200**, 274 (2016).

[58] E. Gull, A. J. Millis, A. I. Lichtenstein, A. N. Rubtsov, M. Troyer, and P. Werner, Rev. Mod. Phys. **83**, 349 (2011).

[59] F. A. Wolf, A. Go, I. P. McCulloch, A. J. Millis, and U. Schollwöck, Phys. Rev. X **5**, 041032 (2015).

[60] A. P. Mackenzie and Y. Maeno, Rev. Mod. Phys. **75**, 657 (2003).

[61] K. S. D. Beach, arXiv:cond-mat/0403055.

[62] G.-Q. Liu, V. N. Antonov, O. Jepsen, and O. K. Andersen, Phys. Rev. Lett. **101**, 026408 (2008).

[63] J. Mravlje and A. Georges, Phys. Rev. Lett. **117**, 036401 (2016).

[64] D. Sutter *et al.*, Nat. Commun. **8**, 15176 (2017).

[65] L. Boehnke, P. Werner, and F. Lechermann, Europhys. Lett. **122**, 57001 (2018).

[66] S. Acharya, D. Pashov, C. Weber, H. Park, L. Sponza, and M. V. Schilfgaarde, Commun. Phys. **2**, 163 (2019).

[67] O. Gingras, R. Nourafkan, A.-M. S. Tremblay, and M. Côté, Phys. Rev. Lett. **123**, 217005 (2019).